Spin Weyl topological insulators

Rafael González-Hernández [*]

Departamento de Física y Geociencias, Universidad del Norte, Km. 5 Vía Antigua Puerto Colombia, Barranquilla 080020, Colombia

Bernardo Uribe [†]

Departamento de Matemáticas y Estadística, Universidad del Norte, Km. 5 Vía Antigua Puerto Colombia, Barranquilla 080020, Colombia

The quantum nature of electron spin is crucial for establishing topological invariants in real materials. Since the spin does not in general commute with the Hamiltonian, some of the topological features of the material can be extracted from its study. In insulating materials, the spin operator induces a projected operator on valence states called the spin valence operator. Its spectrum contains information with regard to the different phases of the spin Chern class. If the spin valence spectrum is gapped, the spin Chern numbers are constant along parallel planes thus defining spin Chern insulating materials. If the spin valence spectrum is not gapped, the changes in the spin Chern numbers occur whenever this spectrum is zero. Materials whose spin valence spectrum is gapless will be denoted spin Weyl topological insulators and their definition together with some of their properties will be presented in this work. The classification of materials from the properties of the spin valence operator provides a characterization which complements the existing list of topological invariants.

I. INTRODUCTION

Topological insulators exhibit a unique electronic structure where the bulk of the material remains insulating due to the presence of a large energy band gap, while the surface or edge states emerge when the material interfaces with a trivial insulator [1,2]. This feature of a material can be related to classical topological invariants associated to the vector bundle of occupied states (valence eigenstates) such as the first Chern number in the 2D case and the Chern-Simons invariant (θ term) in the 3D case [3–5].

The characterization of the topological nature of a material from first-principles calculations has been extensively studied, and several procedures have been established to extract its features, such as Wilson loop calculations [6,7], eigenvalues of crystal symmetry operators [8,9], and elementary band representation of valance bands [10,11]. In this work we propose an alternative strategy to detect the topological nature of a material which is based on the topological properties of the spin operator. The noncommutativity of the spin operator with the Hamiltonian permits us to infer relevant information of the material from the spectrum of the spin operator once it is restricted to the valence bands [12]. The geometrical and topological properties of this spectrum follow the same structural behavior as the ones from the energy spectrum [13,14]. Gapless systems will then have Weyl points (spin Weyl points), and the understanding of the location and the chirality of these points is the key ingredient underlying our proposal for a new indicator.

Our proposal for an indicator enhancing the known classification of topological materials is called the spin invariants vector. This vector has seven integer numbers where the first number counts the number of spin Weyl points with positive chirality and the next six are the Chern numbers of the negative spin valence eigenvalues across the planes $k_l = 0, \pi$ for $l = x, y, z$. The first number is denoted the spin Weyl indicator and it is zero only when the spin valence spectrum is gapped. In this case the spin Chern numbers are constant across parallel planes and the next six coordinates simply encode these constant Chern numbers; in this case the material is a spin Chern insulator when some Chern number is nonzero, or a spin insulator if all Chern numbers are trivial. If the spin Weyl indicator is not zero, then the spin valence spectrum is gapless and the Chern number across parallel planes may differ; we call these materials spin Weyl topological insulators. The next six coordinates provide the information of the Chern numbers across the six planes $k_l = 0, \pi$, and the spin Weyl indicator measures the total positive change of Chern number across parallel planes.

The parity of the spin Weyl indicator is precisely the Fu-Kane-Mele invariant, and in the case of the spin Weyl indicator being even, it provides an enhancement for the detection of weak and fragile topological phases [15].

In order to understand the features of the spin invariants vector, we analyze the behavior of the spin valence operator in the 3D Bernevig-Hughes-Zhang (BHZ) model [16], as well as in particular the tight-binding Hamiltonian [17]. In the 3D BHZ model we obtain five different topological phases depending on one parameter: two trivial insulator phases, two strong topological insulator phases, and one spin Weyl topological insulator phase. This last phase exhibits a gapless spin valence spectrum with a total of four spin Weyl points. Its topological nature is also inferred from the change of spin

*rhernandezj@uninorte.edu.co
†bjongbloed@uninorte.edu.co

Chern number from -1 in $k_z = 0$ to 1 in $k_z = \pi$ (see Fig 2). The tight-binding Hamiltonian exhibits a strong topological insulator phase with two Weyl points and with spin invariants vector $(1|10 - 1000)$. Finally, we calculate the properties of the spin valence spectrum in materials Bi_2Te_3, Bi, and SnTe, thus characterizing Bi_2Te_3 as a strong topological insulator, Bi as a spin Chern insulator, and SnTe as a spin Weyl topological insulator. All three materials exhibit a nonzero spin Hall effect, suggesting that the appearance of the phenomenon is predicted by the nontriviality of the spin Chern numbers.

The spin Chern numbers thus become a customized tool for the distinction and classification of topological insulators. This ansatz was originally put forward by Prodan [12] who showed the robustness of the spin Chern numbers and carried out an extensive analysis of the properties of the spin valence spectrum. The implications of the robustness of the spin Chern numbers have been explored by other authors [18], and in the case of 3D insulating materials, a comprehensive analysis of both theoretical and computational aspects has been studied by several authors [19,20]. By introducing nested spin-resolved Wilson loops and layer constructions, Lin *et al.* [20] studied the behavior of the spin Chern numbers across parallel planes in the BZ, thus describing topological properties of these numbers while detecting the presence of spin Weyl points. This analysis allowed Lin *et al.* [20] to propose a novel method for further classifying topologically insulating phases.

In the present paper we further explore the properties of the spin valence spectrum in 3D insulating materials and we propose an indicator that can effectively identify 3D topologically insulating phases. This newly established indicator, based on the spin properties, offers valuable insights into the fundamental understanding and potential applications of topological materials.

II. INVARIANTS OF TOPOLOGICAL INSULATORS

The mathematics behind the theory of topological invariants in insulating materials has been extensively studied [21,22]. Several methods for detecting topological invariants of a prescribed Hamiltonian have been established and the construction of a comprehensive list of all possible indicators for such invariants is currently an active area of research [23,24].

The importance of these topological invariants lies in the amazing relation that some of them have with certain electromagnetic properties of materials. For instance, in 2D insulators, the Chern number of the occupied states provides the quantization of the anomalous Hall effect [25], and in 3D insulators with time-reversal symmetry (TRS), the nontriviality of the Fu-Kane-Mele invariant (FKM) provides an indicator of a strong topologically insulating type [26], just to mention a few.

The main line of thought underlying the existence of the topological invariants in insulators goes as follows. The Hamiltonian of the periodic system provides a Hermitian operator acting on parametrized vectors over the Brillouin zone (BZ):

$$\widehat{H} : \Gamma(\mathbb{C}^N \times B) \rightarrow \Gamma(\mathbb{C}^N \times B). \tag{1}$$

Here N is the number of bands, B denotes the BZ, and Γ denotes the space of sections of the trivial complex vector bundle $\mathbb{C}^N \times B$.

Whenever there is an energy gap at the Fermi level on the eigenvalues of the Hamiltonian, we say that the material is insulating. The insulating condition permits us to separate the valence states from the conducting ones. This separation at the level of vector bundles defines the partition

$$\mathbb{C}^N \times B \cong E^{\text{val}} \oplus E^{\text{cond}}, \tag{2}$$

where the sections of the bundle E^{val} are generated by the valence eigenvectors of the Hamiltonian $\{|\psi_i\rangle\}_{i=1}^{n_{\text{occ}}}$, where n_{occ} indicates the number of occupied bands which is the rank of E^{val}.

Since E^{val} is a complex vector bundle over the BZ, we may assign to it the topological invariants that it defines in the complex K-theory groups. The only interesting invariant that appears here, besides the rank of the vector bundle, is the first Chern class. This first Chern class $c_1 := c_1(E^{\text{val}})$ can be evaluated on planes inside the BZ and the associated numbers can be determined.

If the first Chern class c_1 is not zero, the material is called a Chern insulator. In the 2D case it provides the quantization of the anomalous Hall effect and several materials exhibit this property [27]. On the other hand, 3D materials with a Chern insulating property have been elusive to detect and until now no single 3D material exhibits this property.

By incorporating geometrical and physical symmetries of the Hamiltonian into the analysis, more specific information regarding the topological invariants can be deduced. If the system preserves TRS ($\mathbb{T}$), and we are in the spin-orbit coupling (SOC) environment with $\mathbb{T}^2 = -1$, then the FKM invariant provides an indicator of the strong topologically insulating property [26,28]. If the symmetry preserved is $C_2\mathbb{T}$, a combination of a 180° rotation and TRS, then an indicator of being an axion insulator is the Stiefel-Whitney class of the $C_2\mathbb{T}$ invariant real vector bundle of E^{val} restricted to the planes fixed by $C_2\mathbb{T}$ [29].

It is important to notice that every extra crystal symmetry will induce topological invariants. Sometimes the invariants already appeared due to another symmetry, but some other times the invariant is new and may or may not imply the existence of invariants of other symmetries. The task of finding a complete set of indicators for all geometrical symmetries is an ongoing subject of research.

Besides the geometrical symmetries, there are also the physical symmetries. These are the ones that come from the fact that we are dealing with a quantum mechanical system. One such symmetry is the spin, and incorporating it into the analysis of topological invariants has been very fruitful [12]. In what follows we will study some of the topological invariants which can be extracted when the spin operator acts in the occupied wave function space.

III. SPIN WEYL INDICATOR

If the spin operator $\widehat{S}_z$ does not commute with the Hamiltonian, we cannot expect to simultaneously diagonalize it with the Hamiltonian. In order to obtain a symmetry of the vector

bundle E^{val}, we compose the action of the spin operator with the projection onto the occupied states:

$$\widehat{S}_z^{\mathrm{val}} : \Gamma(E^{\mathrm{val}}) \to \Gamma(E^{\mathrm{val}}), \tag{3}$$

$$\varphi \mapsto \pi^{\mathrm{val}} \circ \widehat{S}_z(\varphi). \tag{4}$$

Here $\pi^{\mathrm{val}} : \Gamma(\mathbb{C}^N \times B) \to \Gamma(E^{\mathrm{val}})$ is the projection operator $\sum_{i=1}^{n_{\mathrm{occ}}} |\psi_i\rangle\langle\psi_i|$.

We call the operator $\widehat{S}_z^{\mathrm{val}}$ the spin valence (SV) operator and one could see it as a physical symmetry of the bundle E^{val} of occupied states. This SV operator can be diagonalized, and its spectrum can be studied with exactly the same tools as the ones used to understand the spectrum of the Hamiltonian. We have used the $\widehat{S}_z^{\mathrm{val}}$ component for the spin operator, but it can be generalized to include other components.

Note that the SV spectrum takes values in the interval $[-1, 1]$ (in $\hbar/2$ units), and moreover, that an eigenvalue of zero means that there is a combination of occupied states whose spin lies completely on the unoccupied states. Hence it is important to measure whether the SV spectrum crosses the zero value or not, and two different scenarios appear (see Fig. 1).

A. Gapped spin valence spectrum

If the SV spectrum is gapped at zero, then we can partition the vector bundle E^{val} into two different vector bundles:

$$E^{\mathrm{val}} \cong E_{s_z^+}^{\mathrm{val}} \oplus E_{s_z^-}^{\mathrm{val}}, \tag{5}$$

where E_+^{val} and E_-^{val} denote respectively the positive and negative SV eigenstates.

The topological invariants associated to these two complex vector bundles are the first Chern classes

$$c_1^{s_z^{\pm}} := c_1\left(E_{s_z^{\pm}}^{\mathrm{val}}\right) \tag{6}$$

and since

$$c_1 = c_1^{s_z^+} + c_1^{s_z^-}, \tag{7}$$

the new invariant is usually defined as half the difference between the two Chern classes:

$$c_1^{s_z} = \frac{1}{2}\left(c_1^{s_z^+} - c_1^{s_z^-}\right). \tag{8}$$

This Chern class is called the spin Chern class, and together with the total first Chern class c_1, determines uniquely the first Chern class of both the positive and the negative SV states.

When TRS is preserved, the vector bundles $E_{s_z^+}^{\mathrm{val}}$ and $E_{s_z^-}^{\mathrm{val}}$ are isomorphic via the antiunitary transformation defined by $\mathbb{T}$. In this case $c_1^{s_z^+} = -c_1^{s_z^-}$ and therefore the spin Chern class $c_1^{s_z}$ is the invariant preserved. In 2D materials whose spin almost commutes with the Hamiltonian, the spin Chern number is a good indicator for the quantum spin Hall effect. These materials are called quantum spin Hall insulators (QSHIs) and they include both functionalized and pristine antimonene and bismuthene 2D materials [30,31].

In 2D systems Chern classes are uniquely determined by the Chern number, namely the integration of the Chern class on the whole BZ, while on 3D systems they are determined by the integrals along all closed surfaces in the BZ. The value of
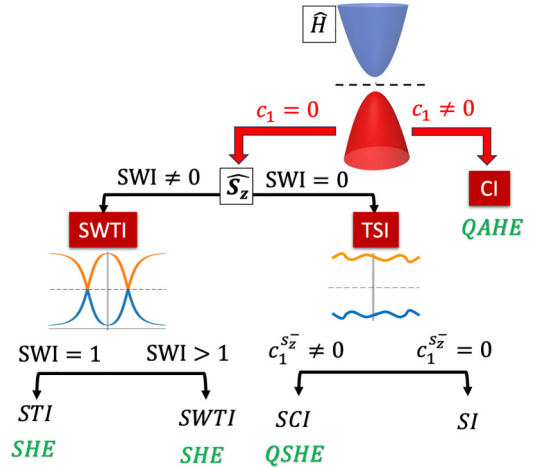

FIG. 1. Topological classification of 3D insulators using Chern classes and the SWI (spin Weyl indicator). If the total Chern class c_1 of the valence states is nontrivial, there is a plane where the Chern number is not zero. In this case the material is a Chern insulator (CI) and the anomalous Hall effect is quantized (QAHE). When the total Chern class of the valence states is trivial, then the SWI number indicates whether the spin Chern numbers vary along parallel planes. Whenever the SWI is trivial, then there are no SW points and therefore the spin Chern numbers do not vary; these materials will be called topological spin insulators (TSIs). In this case if the spin Chern class $c_1^{s_z}$ is trivial, the material is a spin insulator (SI); otherwise the material is a spin Chern insulator (SCI) and has a quantized spin Hall effect (QSHE). Whenever the SWI is not zero, the spin Chern numbers vary along parallel planes and therefore the spin Chern numbers along the planes $k_l = 0, \pi$ do not constitute a complete topological indicator of the material. The case of the SWI being 1 corresponds with most models whose FKM invariant is nontrivial; these are the strong topological insulators (STIs). Materials whose SWI is nontrivial will be denoted spin Weyl topological insulators (SWTIs); these materials show a spin Hall effect (SHE) inside the energy band gap.

this integral over any closed surface surf is the Chern number associated with the surface:

$$c_1^{s_z^{\pm}}(\mathrm{surf}) := \int_{\mathrm{surf}} c_1\left(E_{s_z^{\pm}}^{\mathrm{val}}\right). \tag{9}$$

The spin Chern numbers are usually associated with planes of the form $k_l = 0, \pi$, and in the case of a gapped SV spectrum, these numbers are constant along parallel planes. The spin Chern number can only vary on parallel planes whenever the SV spectrum is gapless, thereby indicating the presence of spin Weyl (SW) points.

B. Gapless spin valence spectrum

Whenever the SV spectrum is not gapped, we cannot partition the occupied states into positive and negative SV eigenvectors all across the BZ. But outside the points in momentum space where the SV eigenvalue is zero, this partition can be performed.

Call *spin Weyl (SW) points* the points in momentum space where there is a zero SV eigenvalue. Around each SW point **k**, a 2D sphere $S_\epsilon(\mathbf{k})$ of small radius $\epsilon > 0$ could be defined.

The vector bundle of occupied states restricted to this sphere splits into positive and negative SV eigenvectors. Therefore we could associate to the SW point the Chern number of the negative SV eigenvectors restricted to the sphere.

Mimicking the definition of the chirality of Weyl points of the Hamiltonian, we define the *spin chirality* of the SW point **k** as follows:

$$\chi^{s_z}(\mathbf{k}) := c_1^{s_z^-}(S_\epsilon(\mathbf{k})).\tag{10}$$

By the Nielsen-Ninomiya theorem [32], the sum of the spin chiralities of all SW points is zero:

$$\sum_{\mathbf{k}\in SW} \chi^{s_z}(\mathbf{k}) = 0,\tag{11}$$

where *SW* denotes the finite set of spin Weyl points in a generic Hamiltonian.

Therefore the maximum Berry curvature flux of the negative SV states is given by the sum of all positive spin chiralities. Simply enclose with a closed surface the spin Weyl points with positive chirality, and by Gauss's law, the total flux is the sum of the chiralities inside the surface.

We claim that this maximum Berry curvature flow of the negative SV states is a topological indicator of the system. We therefore propose to define the *spin Weyl indicator* (SWI) of the system as the sum of the positive chiralities of all SW points:

$$\text{SWI} := \frac{1}{2}\sum_{\mathbf{k}\in SW} |\chi^{s_z}(\mathbf{k})|.\tag{12}$$

The formula above simply computes the sum of the absolute value of all chiralities and divides by two. This way there is no need to distinguish the positive chiralities from the negative ones.

The SWI is a natural number that encodes topological information about the system. For instance, in the presence of TRS or TRS composed with a 2-fold rotation, the parity of the SWI is respectively equivalent to the FKM invariant [26,28] or to the value of the θ term [29]. Whenever the SWI is zero, the projected spin operator is gapped, and the material can be classified as a spin Chern insulator if any spin Chern number is not zero. Whenever SWI is even, the material might be endowed with weak or fragile topological phases.

Calculating the SWI by detecting the SW points together with their chiralities might be cumbersome. Alternatively, we propose to calculate the Chern number of the negative SV eigenstates across planes perpendicular to a given axis. By choosing the k_l axis for $l = x, y, z$ we calculate and plot the function

$$\text{SCN} : [-\pi, \pi] \to \mathbb{Z},\tag{13}$$

$$t \mapsto c_1^{s_z^-}(k_l = t).\tag{14}$$

This function increases and decreases by integer values whenever SW points are crossed, and the total amount of positive changes is precisely the SWI. We will call this function the signal of the *spin Chern number* (SCN); cf. [19].

The SCN signal has been plotted in the 3D Bernevig-Hughes-Zhang (BHZ) model in Fig. 2, in the tight-binding (TB) model of pristine pyrochlore in Fig. 4(c), and in real

materials Bi$_2$Te$_3$ and SnTe in Figs. 5(c) and 5(c'), respectively. In all these cases the value of the SWI can be deduced from the signal of the SCN in the BZ.

C. Spin invariants vector

It is important to notice that the SWI cannot be deduced solely from the spin Chern numbers of the planes $k_l = 0, \pi$ with $l = x, y, z$. The material SnTe has spin Chern number equal to 2 along the planes $k_l = 0, \pi$ for $l = x, y$ and 0 along the planes $k_z = 0, \pi$ [see Fig. 5(c')], while its SWI equals 8.

A coherent set of invariants associated with the SV operator should therefore include the spin Chern numbers along the preferred planes plus the value of the SWI. Hence we propose to define the *spin invariants vector* as the array of seven integer numbers

$$(n|n_x^0, n_x^\pi, n_y^0, n_y^\pi, n_z^0, n_z^\pi),\tag{15}$$

where $n = \text{SWI}$ and $n_l^w = c_1^{s_z^-}(k_l = w)$.

The spin invariants vector will provide the information necessary to determine the spin topological classification presented in Fig. 1. The zero vector represents a spin insulator, a vector with $n = 0$, which is moreover nontrivial, represents a spin Chern insulator, and a vector with $n \neq 0$ represents a spin Weyl topological insulator.

IV. 3D BHZ MODEL

The 2D Bernevig-Hughes-Zhang (BHZ) two-band model [upper left 2×2 matrix of (16)] for a spin topological insulator [16] can be used to construct a four-band Hamiltonian in 3D where two opposite copies of the 2D BHZ model are superposed [matrix of (16) with $D = 0$]. In order to obtain a change of phase for the 2D layers, an off-diagonal term D depending on k_z is added thus obtaining one version of the 3D BHZ Hamiltonian

$$H_{\text{BHZ}}(\mathbf{k}) = \begin{pmatrix} M & A & 0 & D \\ A^* & -M & D & 0 \\ 0 & D & M & -A^* \\ D & 0 & -A & -M \end{pmatrix},\tag{16}$$

where

$$M = M_0 - B_0[\cos(k_x) + \cos(k_y) + \cos(k_z)],\tag{17}$$

$$A = A_0[\sin(k_x) + i\sin(k_y)],\tag{18}$$

$$D = D_0\sin(k_z).\tag{19}$$

This Hamiltonian is written in a basis given by the states $|F\uparrow\rangle, |H\uparrow\rangle, |F\downarrow\rangle, |H\downarrow\rangle$, in that order, and it models a phase transition of a 2D topological insulator. In what follows we will show that changes in the value of $\frac{M_0}{B_0}$ induce five different insulating phases for this 3D model, where each phase change is marked by the closure of the energy band gap.

For $3 < |\frac{M_0}{B_0}|$ it is a trivial insulator, for $1 < |\frac{M_0}{B_0}| < 3$ we have a strong topological insulator (STI) whose SWI is 1, and for $-1 < \frac{M_0}{B_0} < 1$ we have a spin Weyl topological insulator (SWTI) whose SWI is 2. These phases are illustrated in Fig. 2.
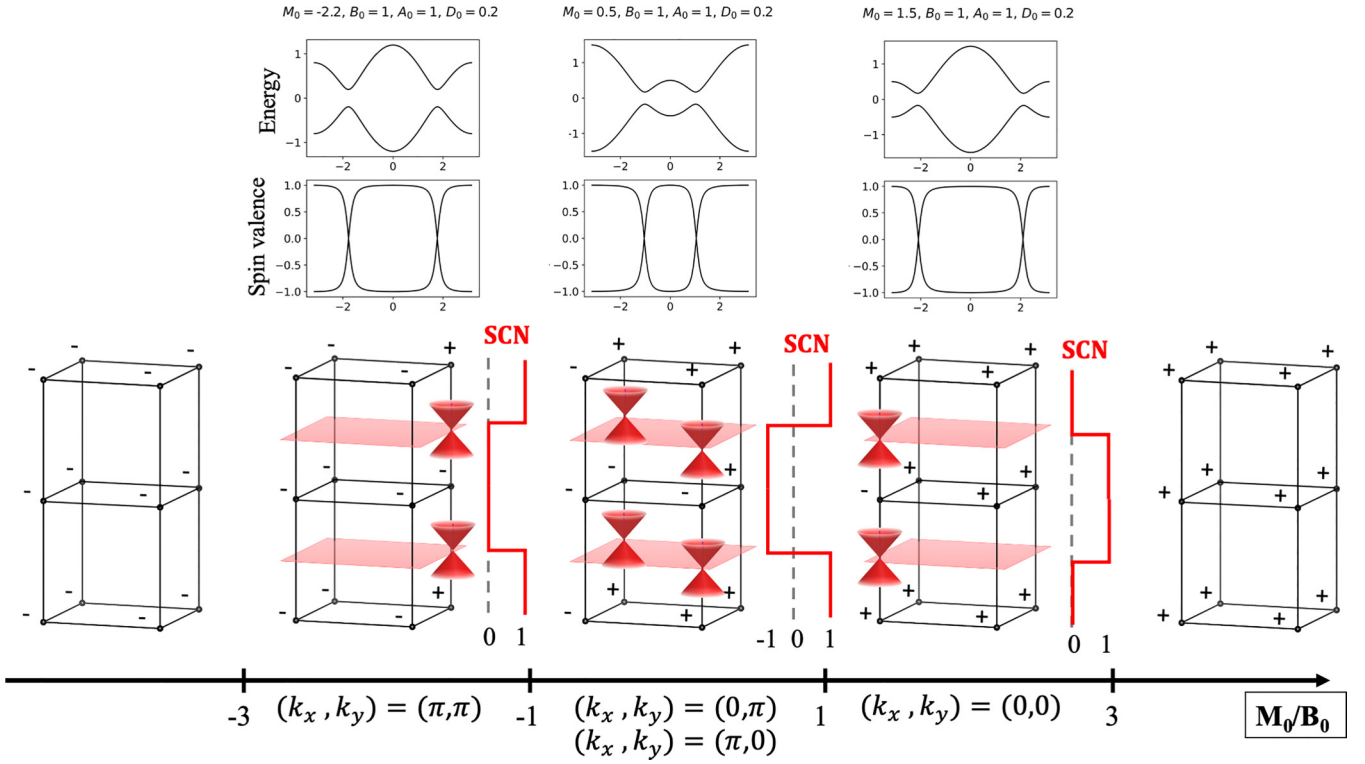
FIG. 2. Five phases of the 3D BHZ Hamiltonian of Eq. (16). For $\frac{M_0}{B_0} = -3, -1, 1, 3$ the Hamiltonian is gapless, and for other values of $\frac{M_0}{B_0}$ the Hamiltonian is gapped. For $|\frac{M_0}{B_0}| > 3$ the system is a trivial insulator, for $1 < |\frac{M_0}{B_0}| < 3$ it is a strong TI with SWI = 1, and for $|\frac{M_0}{B_0}| < 1$ it is a SWTI with SWI = 2. The cones are located where the spin valence eigenvalues are zero, and this occurs along the axis parallel to the k_z axis: in the first nontrivial phase they are on $(k_x, k_y) = (0, 0)$, on the second nontrivial phase on $(k_x, k_y) = (0, \pi)$ and $(k_x, k_y) = (\pi, 0)$, and on the third nontrivial phase on $(k_x, k_y) = (\pi, \pi)$. The signs on the TRIMs denote the eigenvalues of the inversion operator on the negative spin valence eigenstate. The step function on the right of each BZ is the plot of the Chern number of the negative spin valence eigenstate on the planes $k_z = t$ when t varies from $-\pi$ to π. The energy and spin valence plots vs the appropriate axis parallel to the k_z axis in the three nontrivial phases are shown for specific choices of structural constants. The spin Weyl points can be seen in all of them.

The degenerate eigenvalues of the Hamiltonian are $E = \pm \lambda$ with

$$\lambda = \sqrt{(M^2 + |A|^2 + D^2)}, \tag{20}$$

and one choice of eigenvectors is

$$v_1 = ((M - \lambda), A^*, 0, D), \tag{21}$$

$$v_2 = (A, -(M + \lambda), D, 0), \tag{22}$$

$$v_3 = ((M + \lambda), A^*, 0, D), \tag{23}$$

$$v_4 = (A, -(M - \lambda), D, 0). \tag{24}$$

The energy spectrum is gapless only when $M = A = D = 0$ and this only happens whenever $\frac{M_0}{B_0} = -3, -1, 1, 3$. For any other choice of $\frac{M_0}{B_0}$ the energy spectrum is gapped.

Note that the valence states v_1 and v_2 are not linearly independent as presented above; nevertheless this simple presentation of the eigenvectors permits us to deduce an important result that it will be outlined in what follows.

A. Spin Weyl points

The spin operator $\widehat{S}_z$ in this case is the diagonal matrix diag$(1, 1, -1, -1)$, and we may restrict the spin operator only to the valence states. If ψ_j are the eigenvectors of the Hamiltonian forming a unitary base (norm one and perpendicular to

one another), then the SV matrix is defined as follows:

$$(M_{s_z})_{ij} = \langle \psi_i | \widehat{S}_z(\psi_j) \rangle, \quad i, j \in \{1, 2\}. \tag{25}$$

The eigenvalues of the SV matrix give us the SV spectrum. Whenever there is an SV eigenvalue gap, we could separate the positive states from the negative states, and we could find the topological invariants for each group of SV eigenstates. Where the SV spectrum is not gapped, a spin Chern number transition occurs in the BZ. Let us show that this indeed is what happens in the 3D BHZ Hamiltonian.

The SV eigenvalues vanish whenever the whole SV matrix vanishes. Note that in this case, we could use the degenerate basis $\{v_1, v_2\}$ of Eqs. (21) and (22) in order to solve the equations

$$\langle v_i | \widehat{S}_z(v_j) \rangle = 0, \quad i, j \in \{1, 2\}. \tag{26}$$

The equations become

$$\langle v_1 | \widehat{s}_z(v_2) \rangle = 2A\lambda = 0, \tag{27}$$

$$\langle v_2 | \widehat{s}_z(v_1) \rangle = 2A^*\lambda = 0, \tag{28}$$

$$\langle v_1 | \widehat{s}_z(v_1) \rangle = (M - \lambda)^2 + |A|^2 - D^2 = 0, \tag{29}$$

$$\langle v_2 | \widehat{s}_z(v_2) \rangle = (M + \lambda)^2 + |A|^2 - D^2 = 0, \tag{30}$$

TABLE I. Topologically nontrivial phases of the 3D BHZ Hamiltonian. The SW points appear on the four k_z axes, and due to TRS, in pairs of opposite chirality. The first and the third phase have nontrivial FKM invariant and SWI of 1, while the middle phase has trivial FKM invariant with a SWI of 2. The vector of spin invariants appears in the last column.

Phase	Spin Weyl points	Spin Chern number	Spin Weyl indicator	FKM invariant	Spin invariants vector
$-3 < \frac{M_0}{B_0} < 1$	$(\pi, \pi, \pm\cos^{-1}(\frac{M_0}{B_0} - 2))$	$c_1^{s_z^-}(k_z = 0) = 0$	SWI = 1	FKM = 1	$(1|000001)$
	$(\pi, \pi, \pm\cos^{-1}(\frac{M_0}{B_0} - 2))$	$c_1^{s_z^-}(k_z = \pi) = 1$			
$-1 < \frac{M_0}{B_0} < 1$	$(\pi, 0, \pm\cos^{-1}(\frac{M_0}{B_0}))$	$c_1^{s_z^-}(k_z = 0) = -1$	SWI = 2	FKM = 0	$(2|0000-11)$
	$(0, \pi, \pm\cos^{-1}(\frac{M_0}{B_0}))$	$c_1^{s_z^-}(k_z = \pi) = 1$			
$1 < \frac{M_0}{B_0} < 3$	$(0, 0, \pm\cos^{-1}(\frac{M_0}{B_0} - 2))$	$c_1^{s_z^-}(k_z = 1) = 0$	SWI = 1	FKM = 1	$(1|000010)$
	$(0, 0, \pm\cos^{-1}(\frac{M_0}{B_0} - 2))$	$c_1^{s_z^-}(k_z = \pi) = 0$			

and therefore $A = 0$ and $M = 0$. The SW points on each of the three nontrivial phases can be seen in Table I. In this Hamiltonian the SW points come in pairs with opposite chirality due to the TRS.

Now let us find the linear expansion on **k** of the SV eigenvalues around the SW points. For this end we need to find an orthonormal basis of the valence states, and instead of doing it in complete generality, we will only calculate the linear k_z expansion centered on the point $(0, 0, \cos^{-1}(\frac{M_0}{B_0}))$ for the phase $-1 < \frac{M_0}{B_0} < 1$.

Restricting the system to $k_x = 0 = k_y$ we find that the valence unitary eigenvectors for the Hamiltonian $H_{\text{BHZ}}(\mathbf{k})$ for $\mathbf{k} = (0, 0, \cos^{-1}(\frac{M_0}{B_0}))$ are

$$\psi_1 = \frac{(M - \lambda, -D, -(M - \lambda), D)}{\sqrt{2(M - \lambda)^2 + 2D^2}}, \quad (31)$$

$$\psi_2 = \frac{(M - \lambda, D, M - \lambda, D)}{\sqrt{2(M - \lambda)^2 + 2D^2}}. \quad (32)$$

The SV matrix becomes

$$M_{s_z} = \frac{(M - \lambda)^2 - D^2}{(M - \lambda)^2 + D^2}\sigma_x = -\frac{M}{\lambda}\sigma_x, \quad (33)$$

where σ_x is the Pauli matrix. Deriving with respect to k_z and replacing $k_z = \cos^{-1}(\frac{M_0}{B_0})$ we obtain the k_z-linear term of the SV matrix:

$$M_{s_z} \sim \frac{B_0}{D_0}\left[k_z - \cos^{-1}\left(\frac{M_0}{B_0}\right)\right]\sigma_x. \quad (34)$$

Note that when D_0 goes to zero, the slope of the SV spectrum goes to infinity, and the anticommutator of the spin and the Hamiltonian goes to zero. This fact is further explored in Fig. 3.

Similar calculations can be performed for the k_x and k_y linear expansions, thus showing that the SV eigenvalues are linear on **k** around the SW points.

When the structural constants are $M_0 = 0$, $B_0 = A_0 = D_0 = 1$, one can show that

$$M_{s_z} \sim k_x\sigma_z + k_y\sigma_y + \left[k_z - \cos^{-1}\left(\frac{M_0}{B_0}\right)\right]\sigma_x, \quad (35)$$

thus implying that the SW points have chirality ± 1 and that the SV operator behaves like a $\mathbf{k} \cdot \mathbf{p}$ Hamiltonian.

B. Zeeman effect

Consider the BHZ Hamiltonian subject to an external magnetic field in the spin direction

$$H(\mathbf{k}) = H_{\text{BHZ}}(\mathbf{k}) + \mathbf{B}\widehat{S_z}. \quad (36)$$

The energy eigenvalues of the two valence states become

$$\lambda = -\sqrt{\pm 2\sqrt{\mathbf{B}^2(M^2 + |A|^2)} + M^2 + |A|^2 + D^2 + \mathbf{B}^2}, \quad (37)$$

and one can see that there are Weyl-type degenerate eigenstates whenever $|A| = 0 = M$. The same relations were found while solving Eqs. (27)–(30) for the position of the SW points in the BHZ Hamiltonian. Therefore the SW points in the BHZ Hamiltonian, in the presence of a strong magnetic field aligned with the spin direction, evolve into energy Weyl points.

C. Spin Weyl indicator

The three nontrivial topological phases of the 3D BHZ Hamiltonian could be read from the amount of SW points present in the system. The first and third phases provide examples of TIs with nontrivial FKM invariants, thus making them
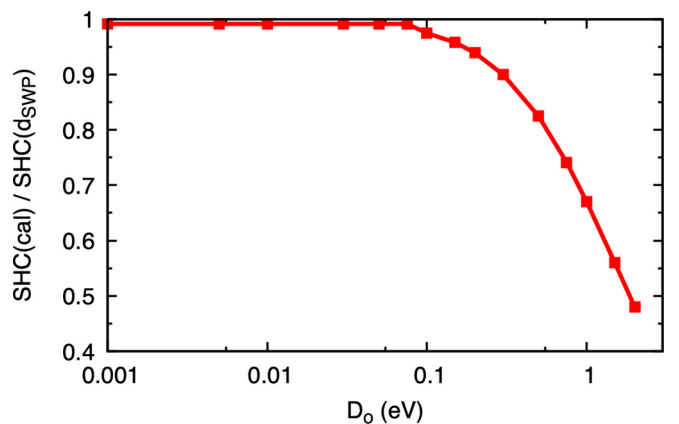

FIG. 3. Spin Hall conductivity calculated with the Kubo formula (40) divided by the spin Hall conductivity calculated from the distance of the SW points in the reciprocal space (38) as a function of the SOC strength D_0 of the 3D BHZ model (16). It is noted that the SHE inside the bang gap is proportional to the SW point distance in the negligible SOC limit.

strong TIs, while the second one has trivial FKM invariant but its SW indicator is equal to 2.

The FKM invariant can be read from the eigenvalues of the inversion operator on the 8 TRIMs. The inversion operator acts via the diagonal matrix diag$(1, -1, 1, -1)$ and the eigenvalues can be seen in Fig. 2. The parity of the number of pairs of negative eigenvalues on the 8 TRIMs is the FKM invariant, and one can see in Fig. 2 that the second phase has trivial FKM invariant. Calculating the first Chern class of the negative SV eigenstates across the planes $k_z = 0$ and $k_z = \pi$ we see that the absolute value of the difference of these Chern numbers is precisely the SWI. The information has been summarized in Table I.

D. Spin Hall effect

It is known that the spin Hall conductivity (SHC) within the energy band gap is a way to classify the charge-spin transport response in topological insulator materials. For 2D TIs, the SHC takes a constant value within the band gap, and in ideal cases like the Kane-Mele model, it becomes quantized (QSHE) [26]. In real materials, the inclusion of SOC induces spin mixing, breaking the commutativity between the spin and Hamiltonian operators, thereby resulting in a nonquantized value for the SHC within the energy gap [33,34]. Despite this fact, the spin Chern numbers [12], and therefore the SWI included in the last section, are well-defined quantities even in the presence of SOC. Therefore, the SWI is a quantity that permits enhancing the characterization of the underlying properties of the system.

In 3D TIs, the characterization of nontrivial SHC within the band gap by topological invariants is still an active area of research. The 3D BHZ Hamiltonian presented above offers a promising model to understand this relation. By performing SHC calculations for the 3D BHZ model (see Fig. 3), we have found that in the limit of minimal spin mixing [corresponding to a small D_0 term in the Hamiltonian (16)], the SHC becomes directly proportional to the proportion of k layers in the reciprocal space with spin Chern numbers equal to 1. This also permits us to detect a relationship between the SHC and the distance between SW points, generalizing the well established relation between the AHE and the distance between energy Weyl points [35]. In the case of the two SW points in the third nontrivial phase of the 3D BHZ model, the SHC inside the band gap can be calculated as [36]

$$\sigma_{ij}^z = -\frac{\hbar}{2e}\frac{e^2 b_z}{2\pi^2 \hbar}, \qquad (38)$$

where $2b_z = 2\cos^{-1}(\frac{M_0}{B_0} - 2)$ is the distance between the SW points in the reciprocal space. When considering the finite spin mixing term in real materials, it becomes evident that the SHC presents a constant and nonquantized value within the energy gap, influenced by the strength of the SOC. This observation is depicted in Fig. 3.

V. TIGHT-BINDING MODEL

The spin Weyl indicator can also be incorporated in tight-binding (TB) models for 3D TIs. We have carried out an extensive calculation on the TB model of the pristine
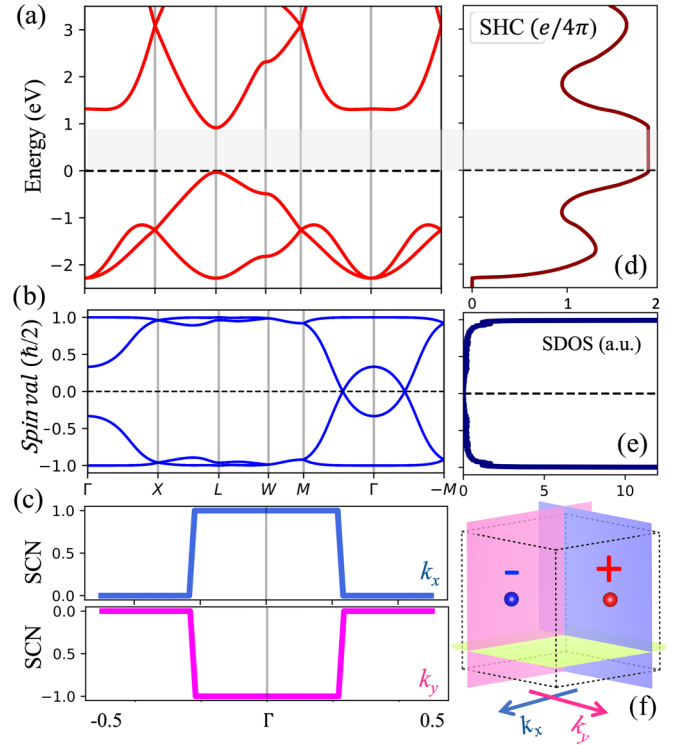

FIG. 4. Tight-binding model introduced in [17] with the Hamiltonian of Eq. (39) and $\lambda = 0.3t$. (a) Bulk band structure and (b) spin valence spectrum along high-symmetry lines in the BZ. (c) Spin Chern number (SCN) calculated for perpendicular planes along the k_x and k_y reciprocal axis, (d) spin Hall conductivity, and (e) spin density of states as a function of the Fermi energy of the tight-binding model. (f) Position of the spin Weyl points in the reciprocal space with the k planes used for the SCN calculation.

pyrochlore model as was introduced by Varnava and Vanderbilt [17]. In this particular case it is well known that the TB model defines a 3D TI and its Hamiltonian has the following form:

$$H = -t \sum_{\langle i,j \rangle, \sigma} \hat{c}_{i\sigma}^\dagger \hat{c}_{j\sigma} + i\lambda \sum_{\langle\langle i,j \rangle\rangle, \alpha\beta} \nu_{ij} \hat{c}_{i\alpha}^\dagger \boldsymbol{\sigma}_{\alpha\beta} \hat{c}_{j\beta}, \qquad (39)$$

where the first term represents the nearest-neighbor hopping interaction, while the second term represents the intrinsic SOC interaction (characterized by the coupling strength λ). In this context, σ_i represents the Pauli matrices, while ν_{ij} is determined by the cross product of $\boldsymbol{b}_{ij} \times \boldsymbol{d}_{ij}$ with $\boldsymbol{d}_{ij}$. Here $\boldsymbol{d}_{ij}$ is the unit vector connecting site i with site j, and $\boldsymbol{b}_{ij}$ is the unit vector from the center of a tetrahedron to the midpoint of the bond $\langle ij \rangle$. This model is exactly the one that appears in Ref. [17], Sec. 3.

This model exhibits a 3D TI that maintains time-reversal and inversion symmetry. By setting the parameter $\lambda = 0.3t$, we computed the band structure at half filling, revealing a band gap of approximately 1.0 eV, as depicted in Fig. 4. We observed the emergence of two SW points along the -M-Γ-M path in the BZ, indicating the presence of these novel spin topological indicators. TB calculations along different k paths revealed that the energy and SV spectrum are gapped in other regions of the BZ.
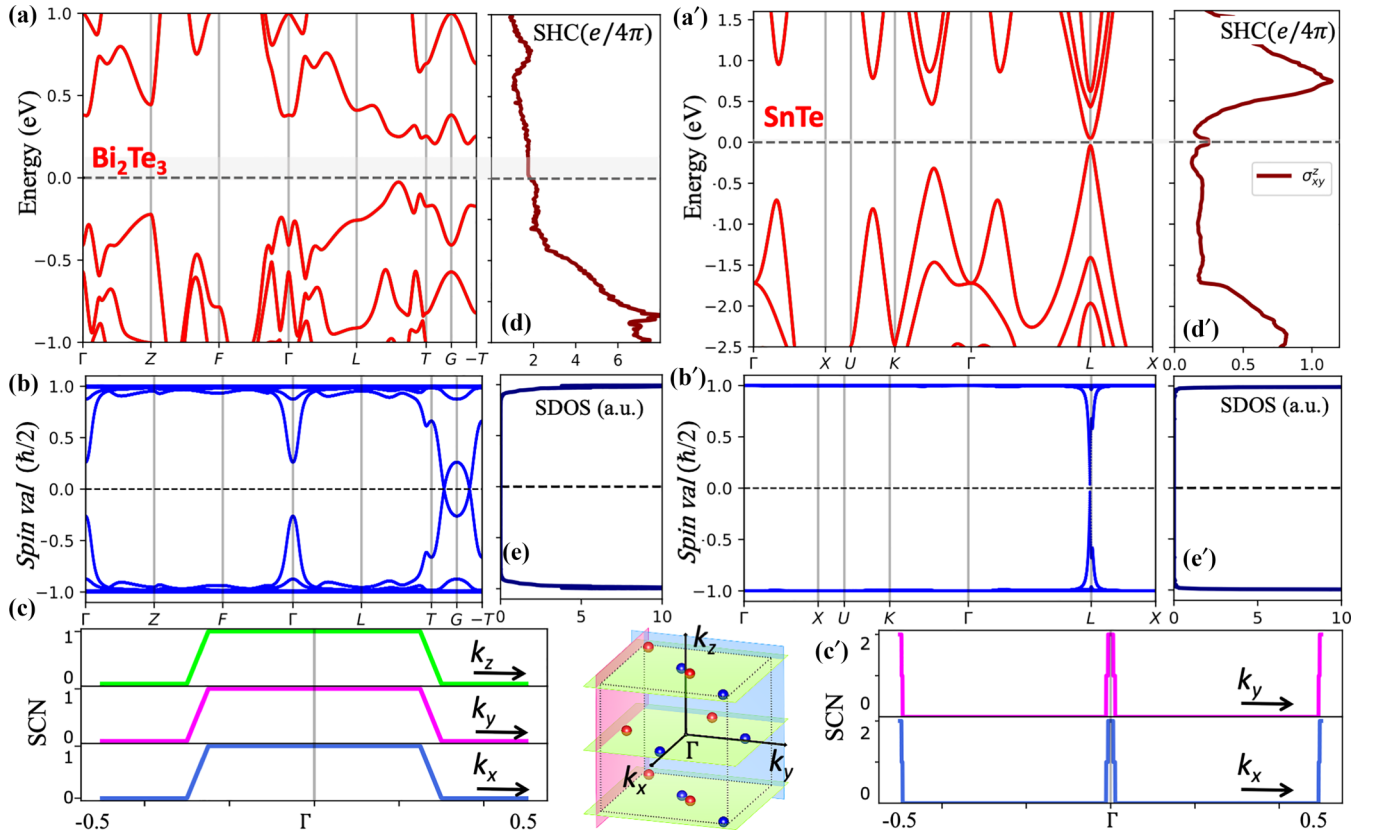
FIG. 5. (a) and (a′) Bulk band structure, (b) and (b′) spin valence spectrum along high-symmetry lines in the BZ, (c) and (c′) spin Chern number—SCN—calculated for perpendicular planes along the k_x, k_y, and k_z reciprocal axis, (d) and (d′) spin Hall conductivity, and (e) and (e′) spin density of states as a function of the Fermi energy of the 3D topological materials Bi_2Te_3 and SnTe. The central panel at the bottom presents the position of the eight SW points of SnTe with their chiralities.

This system exhibits a spin Chern number transition along planes perpendicular to both the k_x and the k_y axis. The presence of SW points in the bulk is inferred from the SCN signal along the k_x and k_y axis as shown in Fig. 4(c). Figure 4(f) depicts the position of the SW points with opposite chirality that produces the SCN signal in the system. This system models a SWTI with SWI = 1, confirming the strong topologically insulating property of the pyrochlore lattice shown in [37,38]. The spin invariants vector for the TB model is (1|10 − 1000).

VI. MATERIALS REALIZATION

We have calculated the spin invariants presented above in real materials, and we have focused our attention on Bi_2Te_3, which is a 3D STI, and SnTe, which exhibits a distinct spin Weyl topologically insulating property. The first material is modeled in a rhombohedral unit cell and consists of two layers of Bi atoms and three layers of Te/Se atoms, arranged in a quintuple layer structure. The coupling between atomic layers within one quintuple layer is strong, but much weaker between two quintuple layers [39]. The electronic band structure of Bi_2Te_3 in the rhomboidal crystal structure is shown in Fig. 5(a). The material exhibits an indirect band gap energy of approximately 0.2 eV.

In the SV spectrum shown in Fig. 5(b) we observe the presence of two SW points along the T-Γ-T k path, corresponding

to the main diagonal of the BZ. As depicted in Fig. 5(e), the spin density of states reveals that the eigenvalues of the spin valence operator are concentrated around ±1 values, except at the SW points. These SW points exhibit opposite chirality and give rise to a transition of the SCN when scanned across perpendicular k planes in the reciprocal lattice. From Fig. 5(c) it is noted that the SCN changes precisely at the positions of the SW points, signifying a topological transition between distinct planes of reciprocal space.

The topological nature of Bi_2Te_3 is evident in our SHC calculation, where a nonzero signal in Fig. 5(d) is observed within the band gap. This material can be classified by a SWI = 1, in agreement with the Fu-Kane-Mele invariant of 1. This indicator is obtained from the calculation of Wilson loops on the $k_l = 0$, π planes, corresponding to 0 and 1, respectively. The position and chirality of the SW points can be inferred from the change of the topological index of 0 at $k_l = 0$ to 1 at $k_l = \pi$ along each k_l direction [see Fig. 5(c)], and its spin invariants vector becomes (1|101010).

On the other hand, the SnTe exhibits a rocksalt crystal structure with two atoms by unit cell [40], and its band gap of around 0.1 eV is located at four equivalent L points within the face-centered-cubic BZ as can be seen in Fig. 5(a′). Despite the trivial FKM invariant calculation predicting a trivial character for SnTe, this material was previously classified as a crystalline topological insulator based on the presence of a nontrivial mirror Chern number [40]. Our findings have been

TABLE II. Spin topology calculated for 3D materials. Spin Weyl points, spin Weyl indicator, Fu-Kane-Mele index, spin invariants vector, time-reversal and inversion symmetry, and spin topology classification according to Fig. 1. Bismuth (Bi) has a constant spin number of 2 along three directions of the BZ. $MnBi_2Te_4$ and $CaMnO_3$ were calculated in the collinear antiferromagnetic phase with Néel vector along the z axis.

Material	SW points	SWI	FKM	Spin inv. vec.	TRS	Inversion sym.	Spin top. class.
Te	0	0	0	$(0\|000000)$	✓	X	SI
GaAs	0	0	0	$(0\|000000)$	✓	X	SI
AuF_3	0	0	0	$(0\|000000)$	✓	X	SI
Bi [41]	0	0	0	$(0\|222222)$	✓	✓	SCI
Bi_2Te_3 [39]	2	1	1	$(1\|101010)$	✓	✓	STI
Bi_2Se_3 [42]	2	1	1	$(1\|101010)$	✓	✓	STI
SnTe [40]	8	4	0	$(4\|222200)$	✓	✓	SWTI
$CaMnO_3$	0	0	0	$(0\|000000)$	X	✓	SI
$MnBi_2Te_4$ [43,44]	2	1	1	$(1\|-1010-10)$	X	✓	STI

corroborated by the observation of a nonzero SHC within the band gap, as shown in Fig. 5(d′).

From the SV spectrum presented in Fig. 5(b′), eight SW points are detected close to the L and T points inducing a change of SCN as presented in Fig. 5(c′). Accordingly, this material is classified by a SWI = 4. The existence of these SW points serves as an indication of the transition in the internal topological phase along the k_x, k_y, and k_z directions. This transition involves a shift from a spin Chern number of 2 at the planes $k_x = 0$ and $k_y = 0$ to 0 in the interior of the interval $(0, \pi)$, to again a shift back to 2 across the planes $k_x = \pi$ and $k_y = \pi$. This feature confirms the SWTI nature of SnTe, but more importantly, it highlights a significant difference from the conventional classification of SnTe using the Fu-Kane-Mele invariant. Here is worth mentioning that knowing the spin Chern number of the system along the planes $k_l = 0, \pi$ is not enough to distinguish its topological nature. In the particular case of SnTe, the spin Chern numbers along the planes $k_l = 0, \pi$ for $l = x, y$ is 2, while along the planes $k_z = 0, \pi$ is 0. One could mistake this material as a SCI, since the spin Chern numbers are equal along parallel planes $k_l = 0, \pi$. Nevertheless, its correct classification is being an SWTI with spin invariants vector equal to $(4|222200)$.

Finally, Table II presents a summary of the 3D trivial and topological insulator materials studied in this work. The table includes the number of spin Weyl points, the spin Weyl indicator, the Fu-Kane-Mele invariant, the spin invariants vector, and the respective (time-reversal and inversion) symmetries associated with each material. We have considered representative examples from different 3D insulator materials to highlight the classification presented in Fig. 1. Te, GaAs, AuF_3, and $CaMnO_3$ display trivial insulator behavior with energy and spin gaps. In contrast, bismuth (Bi) exhibits a constant spin Chern number of 2 along three directions in the BZ, indicating its classification as a spin Chern insulator. This is consistent with previous theoretical investigations that have demonstrated the presence of a 3D topological band structure in Bi [41].

The spin Weyl indicator confirms that the material Bi_2Se_3 exhibits a strong topological character similar to Bi_2Te_3, consistent with previous theoretical and experimental studies [39,42]. Finally, material SnTe exhibits a spin Weyl topological insulator property having eight SW points in the bulk;

and whose distribution can be seen in the central-bottom panel of Fig. 5. This material has a trivial FKM invariant but Fig. 5(d′) shows that it exhibits a nonzero SHC inside the band gap. Therefore we claim that the SWI is more suited to detect SHC signals in 3D topological insulator materials.

Here it is worth mentioning that the properties of the spin Chern number and spin Weyl points in topological insulators remain valid when TRS invariance is broken. This is shown in the case of $CaMnO_3$ and $MnBi_2Te_4$, where the collinear antiferromagnetic phase with Néel vector along the z axis was considered (see Table 1). The topological invariant vector confirms the predicted topological response in $MnBi_2Te_4$, as reported in previous works [43,44].

VII. COMPUTATIONAL DETAILS

We used density-functional theory (DFT) calculations to investigate the spin topology of magnetic and nonmagnetic materials. The generalized gradient approximation (GGA) [45], as implemented in the Vienna *ab-initio* simulation package (VASP) [46], was used to account for exchange and correlation effects. In the electronic structure calculations, we expanded the electron wave function in plane waves with a cutoff energy of 520 eV. The Brillouin zone was sampled using a k mesh of 0.03 $(2\pi/\text{Å})$ k-space resolution. The lattice constants for the studied materials were obtained from the Materials Project database [47].

We employed the wannier90 code to build the maximally localized Wannier basis [48] as a postprocessing approach following the DFT calculations. The pythtb-wannier90 interface of the pythtb code [49] was utilized to generate tight-binding Hamiltonians for the TB model and for each material. Next, we used the electron wave functions of the valence states to generate the spin valence matrix operator and performed its diagonalization to obtain the spin valence spectrum. To study the spin topological properties, we used the spin valence eigenvectors to integrate the Berry curvature (berry-flux utility in pythtb) [49] over 2D k planes, thereby extracting spin Chern numbers across the Brillouin zone. The workflow of this method is shown in Fig. 6.

The intrinsic spin Hall conductivity was calculated using the WannierBerri code [50] by integrating the spin Berry
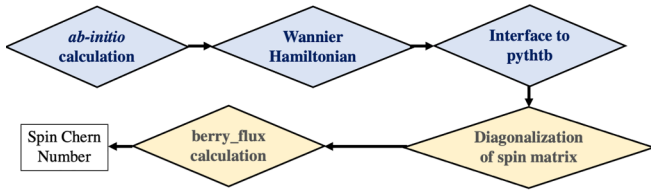
FIG. 6. Workflow showing the computational method. *Ab initio* calculations (VASP code) are used to find the electronic structure of the material. Subsequently, the wannier90 code is utilized to construct the Wannier Hamiltonian, which serves as a basis for the generation of the tight-binding model using the pythtb-wannier90 interface. The next step involves the generation of the spin matrix operator for valence states, followed by its diagonalization to obtain the spin valence spectrum. Finally, the Berry curvature is integrated over 2D k planes to determine the spin Chern number.

curvature over the first Brillouin zone. For the case of SHC (σ_{xy}^z) we set

$$\sigma_{xy}^z = -\frac{e^2}{\hbar} \sum_n \int_{\text{BZ}} \frac{dk^3}{(2\pi)^3} f_n(k) \Omega_{xy}^z(k), \qquad (40)$$

where $f_n(k)$ is the Fermi-Dirac distribution and the Berry curvature $\Omega_n^z(k)$ for the nth band is

$$\Omega_{xy}^z(k) = -2\hbar^2 \text{Im} \sum_{m \neq n} \frac{\langle \psi_n | \hat{j}_x^z | \psi_m \rangle \langle \psi_m | \hat{v}_y | \psi_n \rangle}{(\epsilon_{n,k} - \epsilon_{m,k})^2}, \qquad (41)$$

where $|\psi_n(k)\rangle$ are the Bloch functions of a single band n, k is the Bloch wave vector, $\epsilon_{n,k}$ is the band energy, $\hat{v}_i$ is the velocity operator in the i direction, and $\hat{j}_x^z = \frac{1}{2}\{\hat{v}_x, \hat{s}_z\}$ is the spin current operator. It is important to note that the $\hat{j}_x^z$ definition does not incorporate the spin torque contributions, which is taken into account when the universal spin current operator is used [51]. Finally, the FKM index was computed using the WannierTools code [52].

VIII. CONCLUSIONS

We have found that 3D topological insulators (TI) can be identified by the presence of spin Weyl points in their spin valence spectrum or by the nontriviality of the spin Chern numbers. Both indicators serve as novel predictors of topologically insulating phases. It is important to note that these phenomena cannot be regarded simply as a stack of two-dimensional states, thus making these indicators truly 3-dimensional. In addition, we have found a correlation between the presence of spin Weyl points in 3D TIs and the topological signal of the spin Hall effect (SHE) for the 3D BHZ model.

We propose the use of the spin invariants vector to enhance the topological classification of 3D materials. This vector contains the information regarding the spin Weyl indicator, and the values of the spin Chern numbers of the negative spin valence eigenvectors across the planes $k_l = 0, \pi$ for $l = x, y, z$. This vector contains the necessary information to distinguish the material as a spin insulator, a spin Chern insulator, or a spin Weyl topological insulator. We have provided an array of materials which exhibit interesting spin topology phases and whose spin invariants vector predicts its topological nature.

The novelty of the spin invariants vector is shown when applied to bismuth and SnTe. In the former case the material exhibits a spin Chern insulating property, while the former shows a spin Weyl topologically insulating property. In both cases, the new invariant permits us to carry out a precise classification of these with regard to their spin properties.

We believe that the spin invariants vector adds information to the characterization of the topological classification of materials, enhancing the known invariants and detecting new spin topological phases. Nevertheless, the relation of the spin invariants vector with the whole package of electromagnetic properties stills needs to be investigated.

[1] M. Z. Hasan and C. L. Kane, *Colloquium:* Topological insulators, Rev. Mod. Phys. **82**, 3045 (2010).

[2] X.-L. Qi and S.-C. Zhang, Topological insulators and superconductors, Rev. Mod. Phys. **83**, 1057 (2011).

[3] D. J. Thouless, M. Kohmoto, M. P. Nightingale, and M. den Nijs, Quantized Hall conductance in a two-dimensional periodic potential, Phys. Rev. Lett. **49**, 405 (1982).

[4] X.-L. Qi, T. L. Hughes, and S.-C. Zhang, Topological field theory of time-reversal invariant insulators, Phys. Rev. B **78**, 195424 (2008).

[5] A. M. Essin, J. E. Moore, and D. Vanderbilt, Magnetoelectric polarizability and axion electrodynamics in crystalline insulators, Phys. Rev. Lett. **102**, 146805 (2009).

[6] A. Alexandradinata, X. Dai, and B. Andrei Bernevig, Wilson-loop characterization of inversion-symmetric topological insulators, Phys. Rev. B **89**, 155114 (2014).

[7] A. Bouhon, A. M. Black-Schaffer, and R.-J. Slager, Wilson loop approach to fragile topology of split elementary band representations and topological crystalline insulators with time-reversal symmetry, Phys. Rev. B **100**, 195135 (2019).

[8] M. Iraola, J. L. Mañes, B. Bradlyn, M. K. Horton, T. Neupert, M. G. Vergniory, and S. S. Tsirkin, Irrep: Symmetry eigenvalues and irreducible representations of *ab initio* band structures, Comput. Phys. Commun. **272**, 108226 (2022).

[9] F. Tang, H. C. Po, A. Vishwanath, and X. Wan, Comprehensive search for topological materials using symmetry indicators, Nature (London) **566**, 486 (2019).

[10] B. Bradlyn, L. Elcoro, J. Cano, M. G. Vergniory, Z. Wang, C. Felser, M. I. Aroyo, and B. Andrei Bernevig, Topological quantum chemistry, Nature (London) **547**, 298 (2017).

[11] L. Elcoro, B. J. Wieder, Z. Song, Y. Xu, B. Bradlyn, and B. Andrei Bernevig, Magnetic topological quantum chemistry, Nat. Commun. **12**, 5965 (2021).

[12] E. Prodan, Robustness of the spin-Chern number, Phys. Rev. B **80**, 125327 (2009).

[13] X. Wan, A. M. Turner, A. Vishwanath, and S. Y. Savrasov, Topological semimetal and Fermi-arc surface states in the electronic structure of pyrochlore iridates, Phys. Rev. B **83**, 205101 (2011).

[14] H. Shapourian and T. L. Hughes, Phase diagrams of disordered Weyl semimetals, Phys. Rev. B **93**, 075108 (2016).

[15] Hoi C. Po, H. Watanabe, and A. Vishwanath, Fragile topology and Wannier obstructions, Phys. Rev. Lett. **121**, 126402 (2018).

[16] B. A. Bernevig, T. L. Hughes, and S.-C. Zhang, Quantum spin Hall effect and topological phase transition in HgTe quantum wells, Science **314**, 1757 (2006).

[17] N. Varnava and D. Vanderbilt, Surfaces of axion insulators, Phys. Rev. B **98**, 245117 (2018).

[18] G. F. Lange, A. Bouhon, and R.-J. Slager, Spin texture as a bulk indicator of fragile topology, Phys. Rev. Res. **5**, 033013 (2023).

[19] H. Araki, T. Fukui, and Y. Hatsugai, Entanglement Chern number for three-dimensional topological insulators: Characterization by Weyl points of entanglement Hamiltonians, Phys. Rev. B **96**, 165139 (2017).

[20] L. Kuan-Sen, P. Giandomenic, G. Zhaopeng, H. Yoonseok, B. Jeremy, P. Shoemaker Daniel, M. Fahad, W. Zhijun, A. Fiete Gregory, J. Wieder Benjamin, and B. Barry, Spin-resolved topology and partial axion angles in three-dimensional insulators, arXiv:2207.10099.

[21] D. Vanderbilt, *Berry Phases in Electronic Structure Theory: Electric Polarization, Orbital Magnetization and Topological Insulators* (Cambridge University Press, 2018).

[22] R. Moessner and J. E. Moore, *Topological Phases of Matter* (Cambridge University Press, 2021).

[23] T. Zhang, Y. Jiang, Z. Song, H. Huang, Y. He, Z. Fang, H. Weng, and C. Fang, Catalogue of topological electronic materials, Nature (London) **566**, 475 (2019).

[24] M. G. Vergniory, L. Elcoro, C. Felser, N. Regnault, B. Andrei Bernevig, and Z. Wang, A complete catalogue of high-quality topological materials, Nature (London) **566**, 480 (2019).

[25] Q. Niu, D. J. Thouless, and Y.-S. Wu, Quantized Hall conductance as a topological invariant, Phys. Rev. B **31**, 3372 (1985).

[26] L. Fu, C. L. Kane, and E. J. Mele, Topological insulators in three dimensions, Phys. Rev. Lett. **98**, 106803 (2007).

[27] K. He, Y. Wang, and Q.-K. Xue, Topological materials: Quantum anomalous Hall system, Annu. Rev. Condens. Matter Phys. **9**, 329 (2018).

[28] L. Fu and C. L. Kane, Time reversal polarization and a Z_2 adiabatic spin pump, Phys. Rev. B **74**, 195312 (2006).

[29] R. González-Hernández, C. Pinilla, and B. Uribe, Axion insulators protected by $C_2\mathbb{T}$ symmetry, their k-theory invariants, and material realizations, Phys. Rev. B **106**, 195144 (2022).

[30] Y. Bai, L. Cai, N. Mao, R. Li, Y. Dai, B. Huang, and C. Niu, Doubled quantum spin Hall effect with high-spin Chern number in α-antimonene and α-bismuthene, Phys. Rev. B **105**, 195142 (2022).

[31] D. Wang, L. Chen, C. Shi, X. Wang, G. Cui, P. Zhang, and Y. Chen, Quantum spin Hall insulator in halogenated arsenene films with sizable energy gaps, Sci. Rep. **6**, 28487 (2016).

[32] H. B. Nielsen and M. Ninomiya, Absence of neutrinos on a lattice: (I). Proof by homotopy theory, Nucl. Phys. B **185**, 20 (1981).

[33] F. Matusalem, M. Marques, L. K. Teles, L. Matthes, J. Furthmüller, and F. Bechstedt, Quantization of spin Hall conductivity in two-dimensional topological insulators versus symmetry and spin-orbit interaction, Phys. Rev. B **100**, 245430 (2019).

[34] S. M. Farzaneh and S. Rakheja, Intrinsic spin Hall effect in topological insulators: A first-principles study, Phys. Rev. Mater. **4**, 114202 (2020).

[35] A. A. Burkov, Anomalous Hall effect in Weyl metals, Phys. Rev. Lett. **113**, 187202 (2014).

[36] Y. Sun, Y. Zhang, C. Felser, and B. Yan, Strong intrinsic spin Hall effect in the TaAs family of Weyl semimetals, Phys. Rev. Lett. **117**, 146403 (2016).

[37] H.-M. Guo and M. Franz, Three-dimensional topological insulators on the pyrochlore lattice, Phys. Rev. Lett. **103**, 206805 (2009).

[38] M. Kurita, Y. Yamaji, and M. Imada, Topological insulators from spontaneous symmetry breaking induced by electron correlation on pyrochlore lattices, J. Phys. Soc. Jpn. **80**, 044708 (2011).

[39] Y. L. Chen, J. G. Analytis, J.-H. Chu, Z. K. Liu, S.-K. Mo, X. L. Qi, H. J. Zhang, D. H. Lu, X. Dai, Z. Fang, S. C. Zhang, I. R. Fisher, Z. Hussain, and Z.-X. Shen, Experimental realization of a three-dimensional topological insulator, Bi_2Te_3, Science **325**, 178 (2009).

[40] T. H. Hsieh, H. Lin, J. Liu, W. Duan, A. Bansil, and L. Fu, Topological crystalline insulators in the SnTe material class, Nat. Commun. **3**, 982 (2012).

[41] F. Schindler, Z. Wang, M. G. Vergniory, A. M. Cook, A. Murani, S. Sengupta, A. Y. Kasumov, R. Deblock, S. Jeon, I. Drozdov, H. Bouchiat, S. Guéron, A. Yazdani, B. Andrei Bernevig, and T. Neupert, Higher-order topology in bismuth, Nat. Phys. **14**, 918 (2018).

[42] H. Zhang, C.-X. Liu, X.-L. Qi, X. Dai, Z. Fang, and S.-C. Zhang, Topological insulators in Bi_2Se_3, Bi_2Te_3 and Sb_2Te_3 with a single Dirac cone on the surface, Nat. Phys. **5**, 438 (2009).

[43] Y. Deng, Y. Yu, M. Z. Shi, Z. Guo, Z. Xu, J. Wang, X. H. Chen, and Y. Zhang, Quantum anomalous Hall effect in intrinsic magnetic topological insulator $MnBi_2Te_4$, Science **367**, 895 (2020).

[44] J. Li, Y. Li, S. Du, Z. Wang, B.-L. Gu, S.-C. Zhang, K. He, W. Duan, and Y. Xu, Intrinsic magnetic topological insulators in van der Waals layered $MnBi_2Te_4$-family materials, Sci. Adv. **5**, eaaw5685 (2019).

[45] J. P. Perdew, K. Burke, and M. Ernzerhof, Generalized gradient approximation made simple, Phys. Rev. Lett. **77**, 3865 (1996).

[46] G. Kresse and J. Furthmüller, Efficient iterative schemes for *ab initio* total-energy calculations using a plane-wave basis set, Phys. Rev. B **54**, 11169 (1996).

[47] A. Jain, S. P. Ong, G. Hautier, W. Chen, W. D. Richards, S. Dacek, S. Cholia, D. Gunter, D. Skinner, G. Ceder, and K. A. Persson, Commentary: The materials project: A materials genome approach to accelerating materials innovation, APL Mater. **1**, 011002 (2013).

[48] A. A. Mostofi, J. R. Yates, G. Pizzi, Y.-S. Lee, I. Souza, D. Vanderbilt, and N. Marzari, An updated

version of wannier90: A tool for obtaining maximally-localised Wannier functions, Comput. Phys. Commun. **185**, 2309 (2014).

[49] Python tight binding open-source package, http://physics.rutgers.edu/pythtb.

[50] S. S. Tsirkin, High performance Wannier interpolation of Berry curvature and related quantities with WannierBerri code, npj Comput. Mater. **7**, 33 (2021).

[51] J. Shi, P. Zhang, D. Xiao, and Q. Niu, Proper definition of spin current in spin-orbit coupled systems, Phys. Rev. Lett. **96**, 076604 (2006).

[52] QuanSheng Wu, ShengNan Zhang, H.-F. Song, M. Troyer, and A. A. Soluyanov, WannierTools: An open-source software package for novel topological materials, Comput. Phys. Commun. **224**, 405 (2018).

[53] See https://hpc.uni-mainz.de.